Journal of Sustainability Science and Management *eISSN: 2672-7226*
Volume 15 *Number* 3, April 2020: 36-50

HISTORICAL SHORELINE TREND ANALYSIS IN THE VICINITY OF EL-HAMMRA PORT AT NORTHWESTERN COAST OF EGYPT

THARWAT SARHAN, NADA MANSOUR, MAHMOUD EL-GAMAL AND KARIM NASSAR*

Mansoura University, Elgomhouria St., Mansoura City, Egypt 35516.

**Corresponding author: Karim.nassar@ejust.edu.eg*

Abstract: This research focuses on shoreline monitoring shift frequency using an image analysis technique by Landsat. The methodology has been used for many years (1985, 1990, 1990, 2000, 2004, 2010, 2015 and 2019) by integrating the Landsat Multi-Temporal Images and the Digital Shoreline Analytics System (DSAS) at El-Hammra Beach in Egypt's northwest coast. Landsat images have been geometrically rectified for quantitative analysis of the coastline delineation. Three DSAS numerical characteristic variables, defined as the Endpoint Rate (EPR), Net Shoreline Movement (NSM), and Linear Regression Rate (LRR), measured shoreline accretion and erosion patterns. NSM's findings indicate that the El-Hammra port's seaside was extremely complex, with eastward high erosion. Nevertheless, due to existing defense, including jetty and jets, moderate accretion was discovered. The corresponding peak rate of beach development was high. On the other hand, the coastline has degraded negatively on the east side of the drift and the accompanying beaches have plummeted.

Keywords: Shoreline change rates, DSAS, and landsat images.

Introduction

Coastal shorelines, the interface between land and sea, change in response to various factors, which may be morphological, climatological or geological in nature. The shoreline geometry refers to the collective behaviour of waves, winds, rivers, tides and physical processes. Erosion and deposition can both act as challenges to coastal communities and coastal infrastructures. Over 80% of the worlds' beaches are suffering from coastal erosion with high rates per year ranging from 1cm/year to 30 m/year, and this evaluates a serious danger to many coastal regions (Addo *et al.*, 2008). Changes (whether long-term or short-term) in the geometry of shorelines are significant in the evaluation of coastal dynamism and the management of coastal areas. Therefore, quantitative analysis of shoreline changes over different years has an essential role in understanding and establishing the processes driving erosion and accretion (Sherman,1993; Estives *et al*., 2011). Shoreline geometry and position are the most basic index to estimate changes in coastal areas. Digital Shoreline Analysis System (DSAS) has been used in evaluating the dynamics of shoreline movements, short and long-time historical time scales. However, it is only by including longer time periods (decades to centuries) of investigation that a wider range of past coastal events, magnitudes, and frequencies can be linked with the shoreline morpho-dynamics (Wolman & Miller, 1960). The Digital Shoreline Analysis System (DSAS) is a GIS tool that can be used to compute change rates of shoreline for a time series from that we can predict the shoreline positions or geometry after years. There are numerous examples of the use of DSAS in the study of coastal behaviour and shoreline dynamics. Qualitative and quantitative analysis of shoreline spatiotemporal variations has been addressed by several studies including that of (Kufogbe, 2011; Anand, 2016; Kermani, 2016; Nandi *et al*., 2016). Locally, this is unlike the Northwestern coast in Egypt, specifically the area of study that will be evaluated in this research. The Western desert Petroleum Company established the Al Hammra port in 1968 on the Coast of the Mediterranean Sea and it's far away, about 120 km from West Alexandria and it is for the reception, storage, and shipment of crude oil produced from the Al-Alamein field

as the first commercial discovery in the Western desert. Currently, the production is from 16 companies operating in the Western desert. The port is situated 15 km from El Alamein traffic station. Its shoreline is protected by some coastal structures. This paper aims to study the effect of coastal structural, climatological, morphological and geological on/in nature. Consequently, the current study analyzes shoreline changes of the Northwestern coast at El-Hammra port for a period of over 34 years (1985–2019) using, Geographic Information Systems GIS and automatic computation Digital Shoreline Analysis System DSAS. This study aims to:
(1) apply semi-automated shoreline extraction techniques of band 5 (2) locate and compute the shoreline erosion and accretion rates using different statistical parameters in DSAS along the study area (3) construct a decision matrix for the present state to enable the Egyptian ministry to solve the current issues along the coast studied. This study will offer a highly reliable tool for evaluating coastal changes that should be taken into account when elaborating on coastal management plans in the Northwestern coast. Moreover, it considered an important coast as it seems to be a semi-natural port with a location of petroleum and oil companies.

Study Area

The area of study selected for applications of shorelines changes is Mersa El-Hamra (El-Hamra Port). The main reason for selecting this zone is that it is the largest area with risks to the main problems like erosion and accretion. It is an important area as because it is the site established for the WEBCO cooperation for oil and petroleum. The site is located on the northwestern Mediterranean Sea coast of Egypt at about 120 km west of Alexandria city at approximate longitudes 28° 49` 57`` to 28° 51` 00`` E and latitudes 30° 55` 28`` to 30° 56` 33`` N. The shoreline of this area is oriented in the North/South direction (N/S) shown in Figure 1. The coastline shape is undulating for the length of 4km. It is interrupted by small rocky headlands, forming small embayment and pocket beaches ranging from 20m to 150m length. Two barriers were constructed a perpendicular to shoreline front of the company's shoreline. First Barrier (Main groin) located in the south was constructed in 2006 with a length of 200m. Second Barrier (Temporary groin) was constructed in 2017 with a length of 150m. Figure 2.

Figure 1: The area of study in 2019, and the digitized shorelines 1985, 1990, 1995, 2000, 2004, 2010, 2015 and 2019

Figure 2: The study area in 2006 with the main groin only and at 2017 with the temporary groin

A former jetty, 120m long, was first built on cylindrical piles in 1967 to provide services for marine oil terminal activities, which was located at a water depth of about 20m. In 1991, besides the navigation function, the jetty was extended offshore to an additional 80 m length to be used, in case of emergency, as a fire-distinguishing tool. Unfortunately in 1996, sedimentation and accumulation of sand suddenly occurred in the whole area. The large embayment which hosts the jetty became filled with carbonate sand and extended up to about 120m offshore. The silted sand was spatially accumulated on both sides of the jetty and continued underwater. This seabed sedimentation process has completely blocked the eight inlets of the caisson and has negatively affected the operation of water pumping used for fire distinguishing. Dredging works were executed in January 2000 to remove the accumulated sand. During September 2002, sedimentation had again taken place and blocked the inlet. Due to the significant importance of permanent shoreline observation, the main purpose of this paper is to show that satellite image processing is a precious resource to extract shoreline change automatically covering large geographical scales as well as long temporal scales.

Hydrodynamic of the Study Area

Continuous records of the waves were calculated by S4DW. It recorded the directional wave spectrum every one hour in a water depth of 10.50 m. The wave data is corrected with respect to the North direction as a datum. The results covering the period from January 2000 to December 2008, monthly throughout the year from 1st of January at 00.00 to 31th of December 23.00. The waves in the study area are seasonal with a predominant direction from the north to the northwest. The low regular waves of 50 cm height with 5-8 sec period were noticed during the season summer season (June to August), with calm waves between October and December. Storms occur per year during winter (November to April) and the predominated wave is 1.00 m wave height and 6-8 sec wave period, and the maximum wave height reaches 2.00 m with the probability of occurrences at least once per year. Currents are from the main environmental dynamic forces. It is the main factor in transporting sediments along the coast. Longshore currents were measured between the breaker line and the shoreline (at water depth ranging from 1.00 to 1.80m). Longshore current directions correspond to the wave action. The high storm waves that happen during the year because of the maximum values of velocity. The measurements were taken using a submerged type of floats. The time (T) of a certain distance (L) was determined by using a stopwatch. Then the velocity (V) equals (L/T) m/sec. Studies on wind speed and direction were conducted monthly from 1979 to 2017. The predominant wind direction (50%-80%) of the year is the NW directions while wind (5%-10%) of the year is from SE and NE directions. The average wind speed is seasonal in intensity being 0.77-9 m/sec in summer and in spring is 3-13 m/sec with a higher speed from the NW direction. Figure 3.

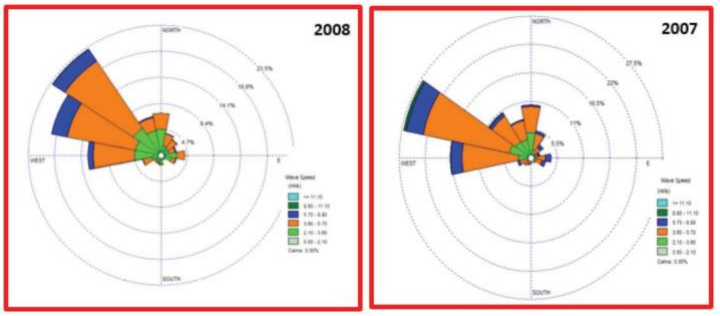

Figure 3: Wave rose along El-Hammra Coast for the years 2007 and 2008

Materials and Methods

Data Source

Due to observable shoreline change, it is important to use a satellite image with good accuracy to monitor these changes. In this research to cover Mersa el-Hammra coast two sources of data are used together to perform analysis and estimation of long-term coastal changes along the coast. Shorelines which were extracted from eight satellite images from 1985 to 2019 (1985, 1990, 1995, 2000, 2004, 2010, 2015 and 2019) are used as well as the measured shorelines and the data of the field for surveying the north western shoreline.

Landsat imagery

Eight imageries were sourced from the USGS Earth Explorer web service scenes. Landsat-1 Multispectral Scanner (MSS), Landsat-4 Thematic Mapper (T M), Landsat-5 Thematic Mapper (T M), Landsat-7 Enhanced Thematic Mapper (ETM), and Landsat-8 Operational Land Imager and Thermal Infrared Sensor (OLI-TRIS) covering a 34-years period from 1985 to 2019 are illustrated in Table.1. They are used to monitor coastal changes along the coastline zone. The tidal range along the Northwestern Mediterranean coast is small. That means the tidal motion did not affect the detected shoreline position using Landsat. All image pre-processing and processing procedures were applied by using Arc GIS 10.1/software package. In addition, automatic shoreline extraction was applied with DSAS. It was developed by the United States Geological Survey (USGS).

Shoreline extraction and Uncertainty Evaluation

In this research, the coastline is called a fluid border between the seaward side and the land side. It can be used as a reference for the evaluation of erosion and accretion processes. The wet/dry line is the most commonly used

Table1: Lists of satellite images used in this study showing their properties

Date of acquisition (Row/Path)	SPACECRAFT_ID	SENSOR_ID	Resolution	Size
1985-1-8	LANDSAT_1	TM	30	178/39
1990-1-16	LANDSAT_4	TM	30	178/39
1995-1-4	LANDSAT_5	TM	30	178/39
2000-1-10	LANDSAT_7	TM	30	178/39
2004-1-5	LANDSAT_7	ETM	30	178/39
2010-1-5	LANDSAT_7	ETM	30	178/39
2015-1-11	LANDSAT_8	OLI_TRIS	30	178/39
2019-1-6	LANDSAT_8	OLI_TRIS	30	178/39

proxy to detect the shoreline position and constitutes a reliable indicator of coastal change for many coastal areas (Smmith, 1990; Anderss, 1991; Sekovski *et al*. 2014; Serrafim, 2017). Shoreline extraction was completed in ArcGIS by the digitization of the dry/wet line identified by pixel values of Landsat imagery. The dry/wet line is defined as the line related to a change in colour/tone between the dry and wet sand. Shoreline extraction from medium resolution satellite images is complex due to the presence of the water-saturated zone at the land-water boundary. In this study, the semi-automatic extraction mechanism was applied by Landsat image Band.5 for each year. The reflectance of water is equal to zero in this wavelength that means the reflectance of other land covers is higher than water. So, the shoreline can be extracted from a single band image, since the reflectance of water is nearly equal to zero to obtain the binary image which considered the first step to extract the shoreline. In this paper, the DSAS was executed in three steps: before anything, we can identify the values of pixels at the image of Band.5 trying to extract the value of shoreline that separates the land from the water. For example, 9000 for the 2019 year (1) Calculate the raster to give the condition value. (2) Convert the raster to polygon. (3) Convert the polygon to line and trying to extract a polyline with one length. The next step is to project the line to real-world coordinate universal transverse Mercator with reference to WGS_1984_UTM_Zone_35N datum. Finally, save the data as shape (.shp) file. We can do that for all the bands each year. Figure 4.

Eventually, the binary image got from each technique in 2019 can be converted into a vector image then extracting the shoreline boundary. The process to select the optimal technique, between the extracted shorelines and the measured ones in 2019 was done in ArcGIS 10.2.2. This analysis is done using DSAS tools in five steps. (1) Shoreline preparation. (2) Baseline creation (Buffering method). (3) Transects generation. (4) Computation of distance difference from baseline and shorelines at each transect, and (5) Calculation of rate of shoreline change. According to these steps, the difference between the extracted and the measured shoreline is calculated on 161 transects generated perpendicular to the baseline. These transects were precisely cast at intervals of 20 m with length of 600m. Transects are numbered from 1 to 161, with transect 1 on the west and transect 161 on the east. Figure 5.

Checking the error between the measured and the digitized shoreline in 2019 for the zone was done and plotted as in Figure 6. In Figure 9-a, it demonstrates the residuals between the measured and the digitized shoreline in 2019 at each transect line from 1 to 161 using the histogram threshold of band 5. Figure 9-b Data points were reasonably distributed on either side of a 45° line which was used for observing the correlation between the transect lengths of the

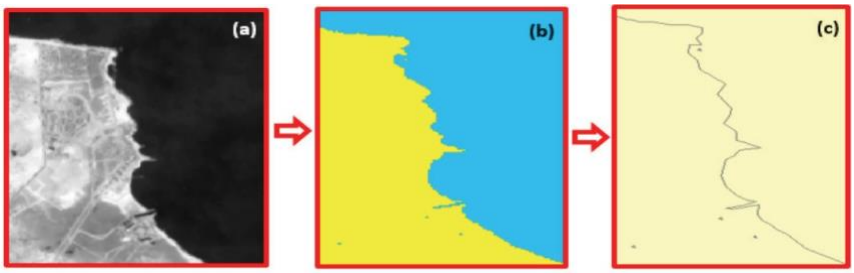

Figure 4: The steps of shoreline extraction for the year 2019. (a) Band.5 from Landsat image. (b) The binary image or raster image which resulted from condition (c) the polygon image which resulted from the conversion of a raster image

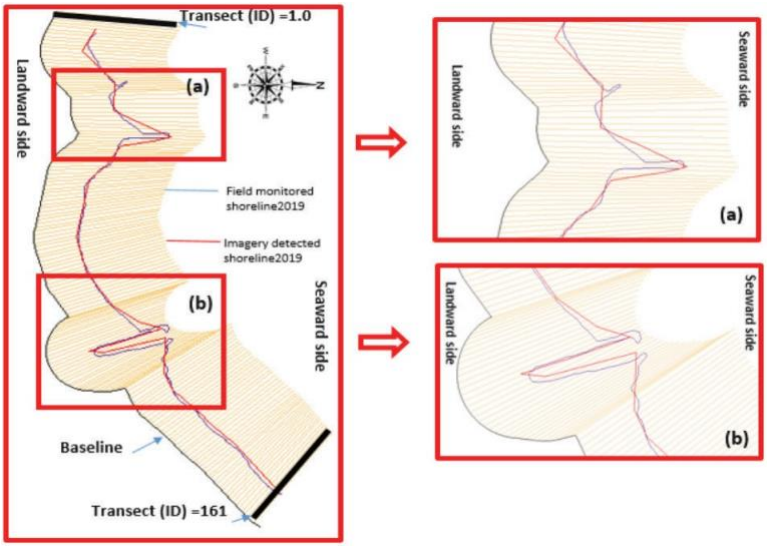

Figure 5: Rapprochement encompasses the digitization of shorelines from field data in 2019 and the corresponding Landsat imagery

measured and imagery detected shoreline for the zone. The normalized root means square error (NRMSE) is selected to determine the optimal shoreline detector technique, as it considers a non-dimensional form of the RMSE as follows (Eqs. (1) and (2)):

$$RMSE = \sqrt{\frac{\sum_{i=1}^{n}(L_{obs,i} - L_{extract,i})^2}{n}}, \qquad (1)$$

$$NRMSE = \frac{RMSE}{L_{\overline{obs}}}, \qquad (2)$$

Where is the number of transects; $L_{obs,i}$ is the transect length from baseline to the observed shoreline at transect number i ; $L_{extract,i}$ is the transect length from baseline to the extracted shoreline at intersect number i and L_{obs} is the average of transects lengths of the observed shoreline. The annualized NRMSE for extracted shorelines over a period of 34 years (1985-2019) calculated by DSAS tools. By calculating the NRMSE for 2010, 2015 and 2019 are 0.110, 0.120 and 0.095 respectively. To reach these values, values, some trials had to be done when identifying the pixel values. For the year 2019 to reach the value of NRMSE 0.095, for the first trial, the pixel value of 9000 was identified to digitize the shoreline, then the value of NRMSE is calculated by the results of transect values by DSAS tools. For the second trial, pixel value of 10000 was identified to digitize the shoreline with NRMSE 0.027. For the third trial, pixel value of 11000 was identified to digitize the shoreline with the value of NRMSE 0.113. Identifying the difference between the measured and the digitized shoreline was done by calculating Residuals that are shown in Figure 6. In addition, Figure 6d shows the frequencies of absolute errors in the actual and measured shoreline of 2019 using different pixel values of the raster image (9000, 1000, and 11000). It is clearly noted that the highest frequency errors do not exceed 5.0 m. While the pixel value of 9000 is the superior for the shoreline extraction.

Change Rate Calculation

Changes of shoreline positions are calculated by DSAS tools using four data analysis techniques (i.e., EPR, LRR, and NSM. The End Point Rate (EPR) is calculated by dividing the difference of distance of shorelines (m) by the time elapsed between the earliest and latest measurements at each transect.as follows Eqs. (3)

$$EPR = \frac{L_1 - L_2}{t_1 - t_2}, \qquad (3)$$

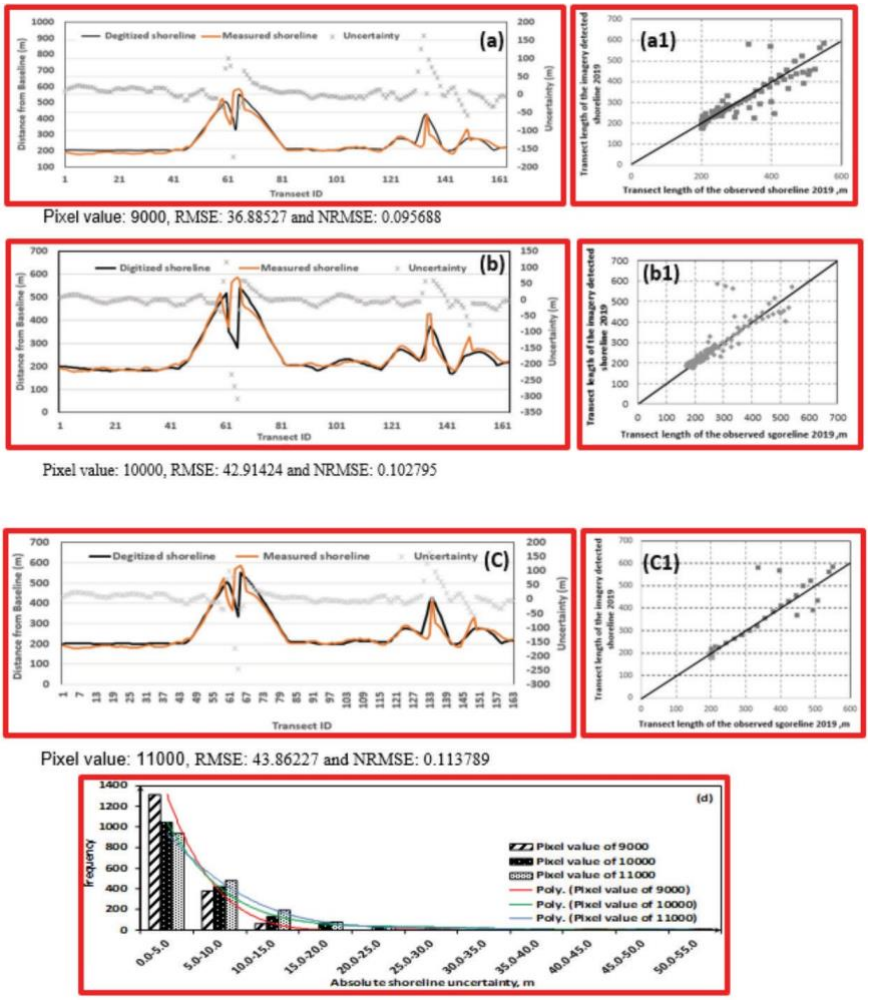

Figure 6: Validation procedure between field-monitored and the imagery-detected shoreline in 2019, (a&a1) represent the pixel value 9000, (b&b1) represent the pixel value 10000, (c&c1) represent the pixel value 11000, and (d) the corresponding frequency error curve

Where, L_1 and L_2 are the distance of shoreline movement (separating the shoreline and baseline); t_1 and t_2 are the dates of the two shoreline positions (the time elapsed between the earliest and latest measurements at each transect).The Least Regression Rate (LRR) this method consists of fitting a least squares regression line to multiple shoreline position points for a particular transect in Figure 7. The shoreline change rate along each transect for all years (i.e., 1985, 1990, 1995, 2000, 2005, 2010, 2015 and 2019) is computed by plotting the points where shorelines are intersected by transects and calculating the linear regression equation, which has the form: $L = b + mx$ where, L: represents the distance (m) from the baseline that constructed by buffering method at a distance of 200m from 2019 extracted shoreline. Shorelines dates interval (years), (m) the slope of fitted line (*m/year*) which considered LRR (shoreline change rate). Shoreline can be classified based on the rate of change as shown in Table.2. (Natesan *et al*., 2015).The sample data are used to calculate a mean offset, and the equation for the line is determined by minimizing this value so that the input points are

positioned as close to regression line as possible. in figure 7.The (NSM) is the net spacing (*m*) between the old and new shorelines position for each intersect (1985-2019). It indicates a distance not a rate. The negative value of EPR, LRR, and NSM indicates landward recession of the shoreline (erosion), while a positive value denotes seaward emigration (accretion).

Finally, the mechanism of shoreline change rate calculation is summarized and consigned in Figure 8.

Results

Analysis of Shoreline Change Rates

In this research is where the coastline was extracted from satellite images for 1985, 1990, 1995, 2000, 2004, 2010 and 2019. The coast-line rate of change was computed using DSAS software. The methodology of shoreline change rates calculation started with the creation of personal geodatabase in Arc-Catalog 10.2.2 for the extracted shoreline positions. Each shoreline has an attributes table which includes date, length, ID, shape, and uncertainty. The date of acquisition for each image is entered in the date column while the length, ID, and shape are automatically generated. Uncertainties are also quantified relay on the year and entered as integers for the uncertainty column. The eight shoreline positions are then appended to one shape-file. Posteriorly, a hypothetical baseline is constructed from the shoreline. There are three methods for constructing baseline: (1) start with a new feature class; (2) buffer an existing shoreline; (3) use a preexisting baseline. The second method is the most reliable and accurate method for constructing a baseline. It takes the same tortuosity shape of the nearest shoreline. Baselines were built in parallel with the general shoreline trend. The baseline is set at a buffering distance of 600 m offshore away from the closest shoreline. Transects as well as the location of the baseline with respect to the shoreline (onshore or offshore). Correspondingly, transects have

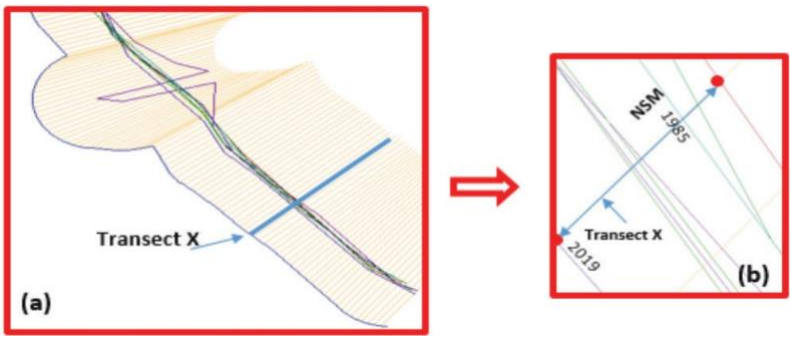

Figure 7: Expository example of NSM, EPR, and LRR. (a) Map of the coastline of Mersa El-Hamra from the east of jetty, with the indication of the transect (x). (b) Details of transect line (x) and shorelines intersection

Table 2: Shoreline classification based on EPR and LRR (Natesan *et al*., 2015)

Category	Rate of shoreline change(m/year)	Shoreline classification
1	>-2	Very high erosion
2	>-1 and <-2	High erosion
3	>0 and <-1	Moderate erosion
4	0	stable
5	>0 and <+1	Moderate accretion
6	>+1 and <+2	High accretion
7	>+2	Very high accretion

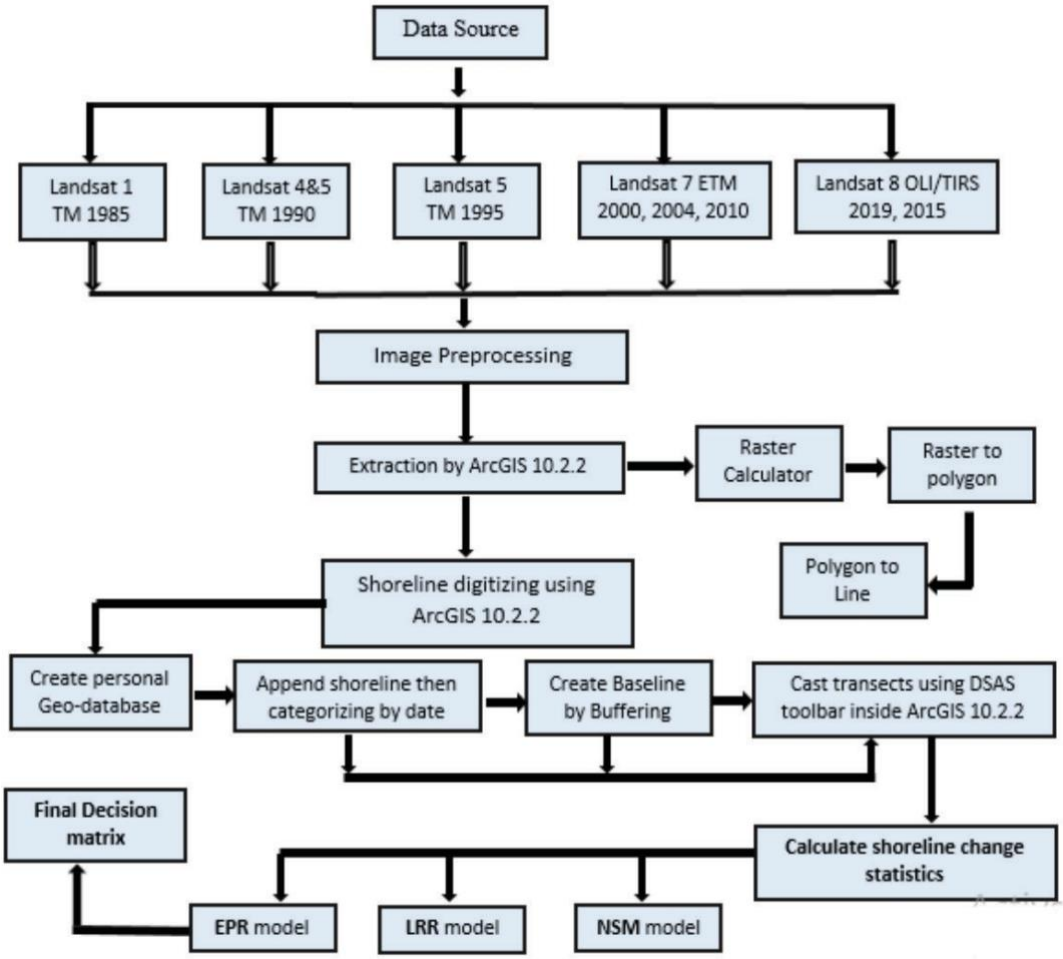

Figure 8: The flow chart of the methodology

been cast orthogonally from the baseline across the shoreline of different years in an interval of 50m after the creation of transects feature class, the change rates of shoreline are automatically calculated by using several statistical models (i.e., EPR, LRR, and NSM) The table shows that statically results are joined related to the transect feature class by the field (Object ID) in the transect feature class. Completing the joining process allows classifying of transect into two categories in the form of erosion (purple transects) and accretion (blue transects) by adjusting the symbology of the transect feature class (Figure 9). The demarcation of erosion and accretion transects indicates that most beaches are subjected to accretion and treat in 1985-2019. This study reveals that during this period 32.40% (23 transects) of the coastline corresponding to 1100 m are in the erosional regime for the zone. (Figure 10) and Table.4. In the same sequence, 67.60% (48 transects) of the coastline with a length of 2350m is in the accretionary regime. (Figure 10) and Table.4. The annualized shoreline change rates are quantified for the study area from 1985 to 2019 using the statistical outputs of EPR, LRR and NSM (Figure (10-b) Figure (10-c)). The results of the present study are gathered and assigned in Table 2; they materialize the mean and maximum rates of coastline progress and regress as well as the percentage of erosion and sedimentation transects. The positive and

negative values of the EPR, LRR, and NSM in Figure (10-b) Figure (10-c) and Table 4 indicate accretion (above the line of zero change) and erosion (beneath the line of zero change) areas respectively. The positive and negative values of the EPR every five years in Table 3 indicate accretion and erosion areas respectively. Figure (10-b) Figure (10-c) show that almost the whole coastal area was subjected to accretion to over a period (34 years). Figure 11 shows the sectors of erosion and accretion in the study area every five years in the last 34 years.

As a result of the analysis, the most significant changes were observed in Table 2. (Natesan *et al*. 2015). Qualitative analysis was done for determining erosion and accretion transects using the EPR model along the shoreline.

Decision Matrices by LRR Model

A decision matrix is a simple method that can be used for making complex decisions. It can be used particularly, in cases where there are many alternatives and many criteria of varying

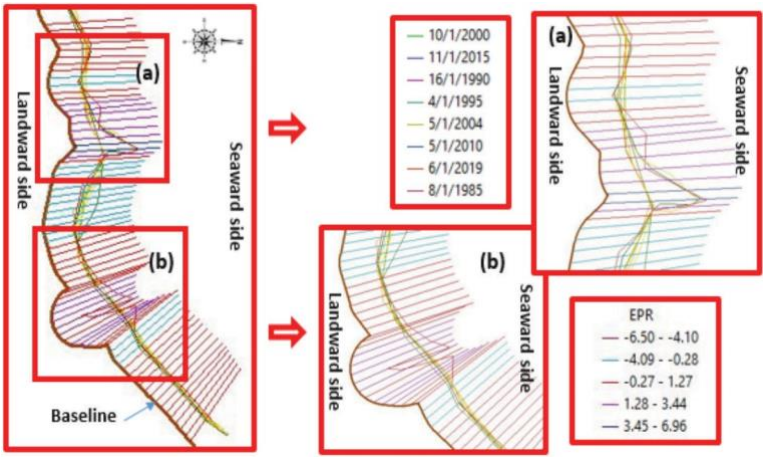

Figure 9: Qualitative analysis for determination of erosion/accretion transects using EPR which functionalized in DSAS based on the digitized shorelines in the years of 1985, 1990, 1995, 2000, 2004, 2010, 2015 and 2019

Table 3: Coastline rate of changes (EPR) every five years during years (1985-2019)

Rate of change EPR (m/yr)	1985-1990	1990-1995	1995-2000	2000-2004	2004-2010	2010-2015	2015-2019
Mean progressive +ve	+1.1947	+2.082	+8.562	+6.115	+5.569	+2.367	+21.86
Mean Regressive -ve	-0.9456	-3.37185	-4.640	-7.087	-3.122	-1.33	-57.52
Maximum progressive +ve	+3.75	+4.86	+30.10	+10.47	+31.54	+7.06	+6.527
Maximum Regressive -ve	-3.95	-12.52	-8.58	-21.95	-0.47	-3.13	-7.817
Total transects that record accretion/*the percent%*	17/*25*	36/*52.94*	28/*41.17*	40/*58.82*	25/*36.76*	43/*63.23*	37/*54.11*
Total transects that record erosion/*the percent%*	50/*73.5*	26/*38.23*	39/*57.35*	24/*35.29*	39/*57.35*	17/*25*	29/*42.64*

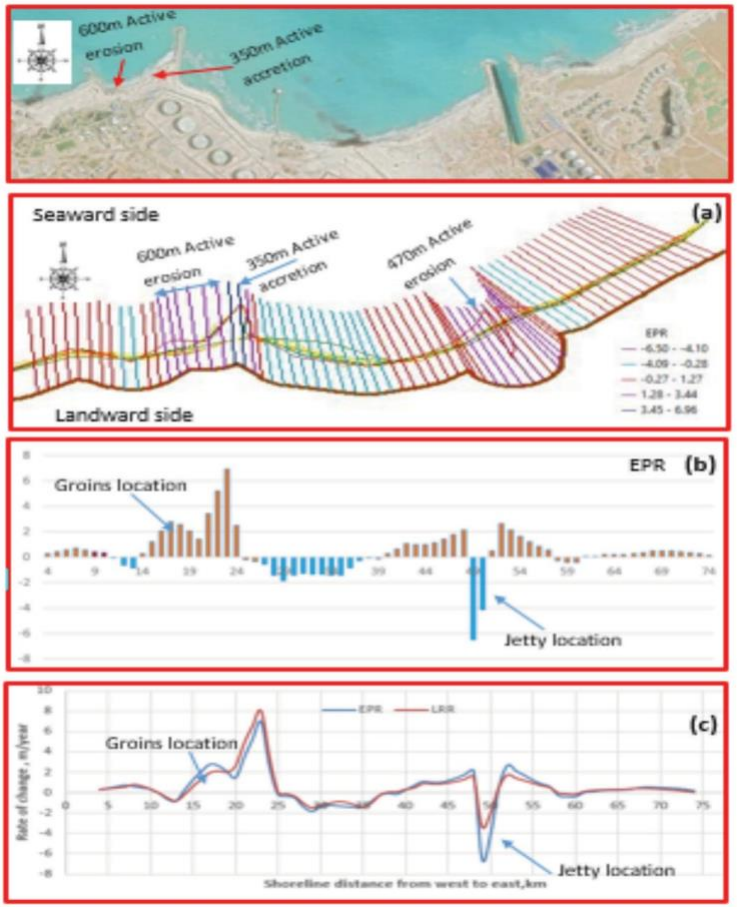

Figure 10: Quantified shoreline change rates by EPR and LRR (m/year) in for the study area (a) by using DSAS tools at (b) then calculating the results of EPR (c) both of EPR and LRR results in one figure (d). All Results during the period from 1985 to 2019

importance to be considered. In the present study, decision matrices have been created based on LRR results in the period of 1985–2019 for the area of study. It can be used as a qualitative and quantitative tool to enable the Egyptian ministry to take appropriate actions for that important coastal zone. The final decision was based on dividing the area of study into a group of regions. The first column is the sector name based on the values of LRR and the second column is the length of the sector. The third is a number of transects that are based on the name of the sector. The fourth is the mean value of LRR for each sector. The fifth is the evaluation of the values of LRR that based on the classification of change rate values that are shown in Table 2. The sixth column illustrated the risk values which classified the risk sensitivity into high, moderate, and low. There are two evaluations and the first was based on the rate of the erosion and accretion and the second has included the risk level of the near-shore land use services liable to erosion and accretion hazards which were practically studied by (Frihy and El-Sayeed, 2013) as they classified the risk sensitivity into high, moderate, and low. In this research, the study area is divided into nine sub-regions (A,B,C,D,E,F,G,H and I) depending on the concavity variation of erosion and accretion, intensity curve plotted by

Table 4: Coastline change trends of the study area during the period between 1985-2019

Mersa El-Hammra Coast from west to east	
Total Number of transects	71 transects
Baseline length (m)	4416.28
NSM mean accretion (m)	+43.34
NSM mean erosion (m)	-39.71
NSM max accretion (m)	+236.57
NSM min accretion (m)	-221.04
Mean Progressive shoreline Change Rate (m/year)	
EPR (End Point Rate)	+1.235
LRR (Least Regression Rate)	+1.205
Mean Regressive shoreline Change Rate (m/year)	
EPR (End Point Rate)	-1.167
LRR (Least Regression Rate)	-0.93
Max Progressive shoreline Change Rate (m/year)	
EPR (End Point Rate)	+6.96
LRR (Least Regression Rate)	+8.04
Max Regressive shoreline Change Rate (m/year)	
EPR (End Point Rate)	-6.50
LRR (Least Regression Rate)	-3.35
Total transects that record accretion/*the percentage*	
NSM (Net Shoreline Movement)	48/*67.60*
EPR (End Point Rate)	48/*67.60*
LRR (Least Regression Rate)	49/*69*
Total transects that record erosion/*the percentage*	
NSM (Net Shoreline Movement)	23/*32.4*
EPR (End Point Rate)	23/*32.4*
LRR (Least Regression Rate)	21/*29.57*

LRR results in Figure 13 and where shorelines exhibiting recession are located at sectors B, D, H and F where jetty located, while accreting shorelines were observed at sectors A, C, E, G, and I. The maximum rate of erosion -2.69 m/year occurs at F sector where the jetty is located. The maximum accretion rate of 3.05 m/year occurs at the C sector where groins are located. The technique of decision for sectors is determined according to the algorithm shown in Figure 12. (K.Nassar *et al.*, 2018)

Conclusion

The port of El-Hammra is known to be a significant oil and petroleum agency, but monitoring of the process of erosion and accretion in this area is crucial. This paper has therefore shown that the application of remote sensing and GIS technologies is crucially relevant with reasonable accuracy in long-term shoreline change studies. For coastal engineering and coastal zone planning, measuring of coastal changes it is necessary to define effective management strategies and recommendations for coastal areas. Accordingly, the efficient

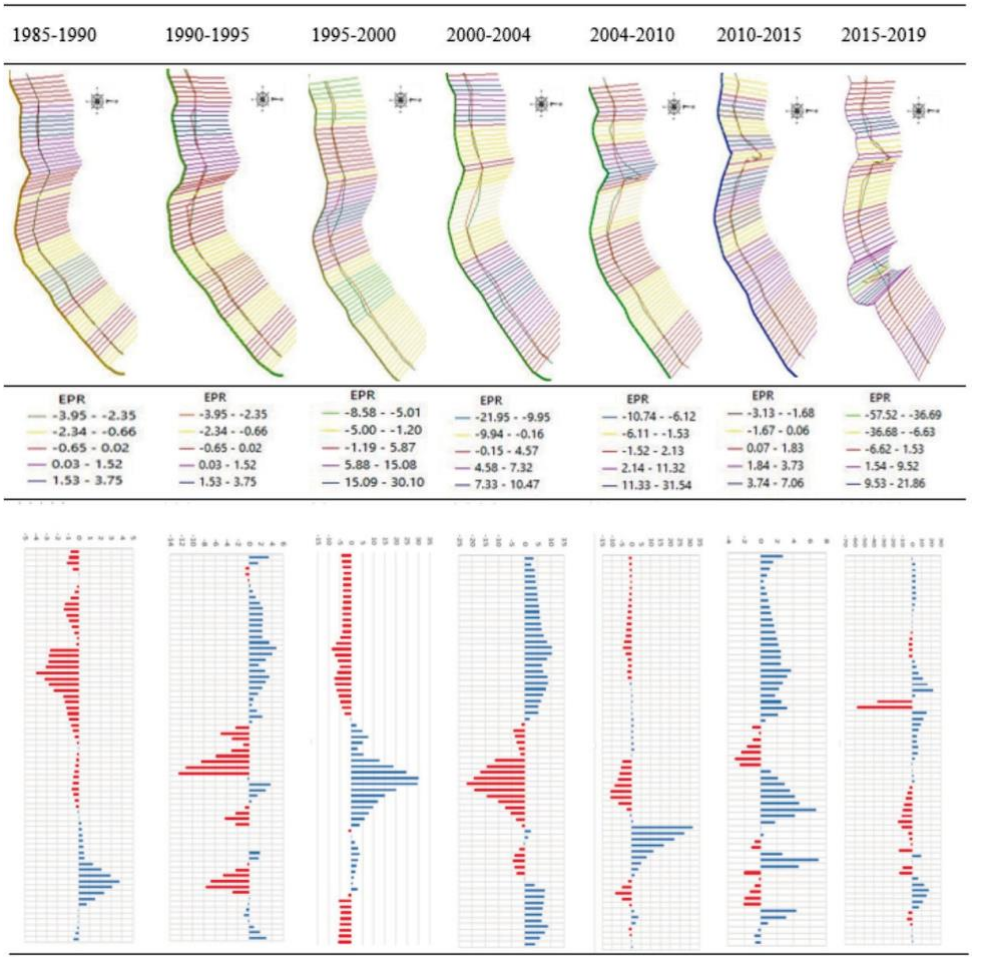

Figure 11: Qualitative analysis for determination of erosion/accretion transects using EPR which was functionalized in DSAS every five years during years (1985-2019) for the study area.
Note : accretion/erosion

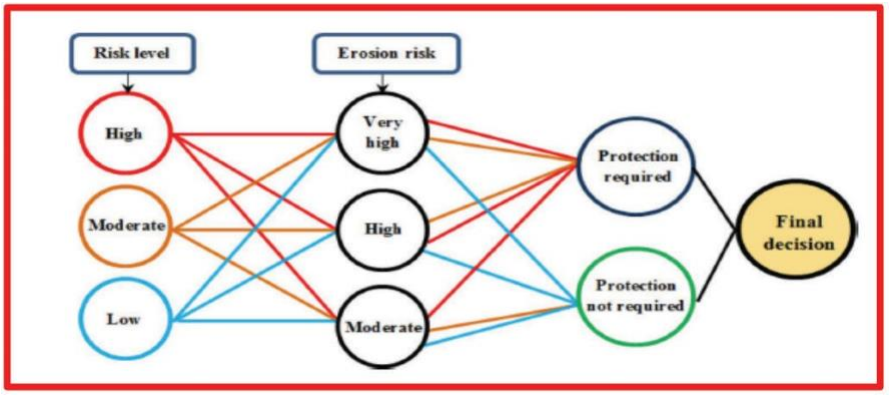

Figure 12: The methodology of decision algorithm (K.Nassar *et al*., 2018)

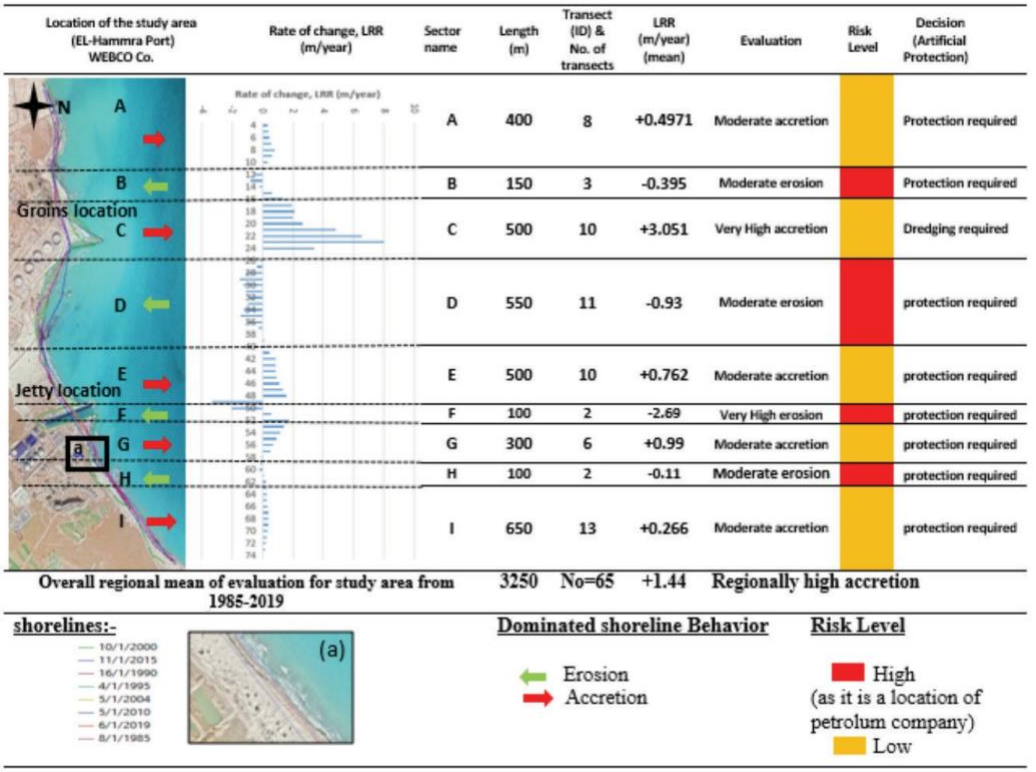

Figure 13: Decision matrix showing shoreline evaluation and risk assessment for the study area by LRR between 1985 and 2019

classification and quantification of the shoreline change in the study area with multi-temporary satellite images over a period of 34 years (1985–2019) require the use of geospatial methodology and automated DSAS calculations. Applying explicitly ArcGIS 10.2.2 with the histogram of band 5, eight shorelines were digitized in 1985, 1990, 1995, 2000, 2004, 2010 and 2019. As a result, the maximum recorded coastal erosion/creation kinematics for the study area is -3.35/+8.04 m/year, based on the current protection system of jetties and groins. The findings of this article also show that the use of Satellite images (medium resolution), GIS and automatic DSAS could be helpful for data on morpho-dynamic coastal zoning and coastal management on Egypt's northwest coast. In the long run, the study provides a highly reliable method for local coastal managers and decision-makers to use the results obtained to assess coastal changes which should be taken into account when designing the coastal management plans for the northwest coast of Egypt.

Acknowledgements

The first author would like to thank and express appreciation to Dr. Mohamed El-Sharabasy, Mansoura University and Dr.Maysara El-Tahan, Alexandria University for their support and for offering the field data needed for this research.

References

Zed, A. A., Soliman, M. R., & Yassin, A. A. (2018). Evaluation of using satellite image in detecting long term shoreline change along El-Arish coastal zone, Egypt. *Alexandria Engineering Journal*, *57*(4), 2687-2702.

Ayadi, K., Boutiba, M., Sabatier, F., & Guettouche, M. S. (2016). Detection

and analysis of historical variations in the shoreline, using digital aerial photos, satellite images, and topographic surveys DGPS: case of the Bejaia bay (East Algeria). *Arabian Journal of Geosciences*, *9*(1), 26.

Ayadi, K., Boutiba, M., Sabatier, F., & Guettouche, M.S. (2016). Detection and analysis of historical variations in the shoreline, using digital aerial photos, satellite images, and topographic surveys DGPS: case of the Bejaia bay (East Algeria). *Arabian Journal of Geosciences*, *9*(1), 26.

El Banna, M. M., & Hereher, M. E. (2009). Detecting temporal shoreline changes and erosion/accretion rates, using remote sensing, and their associated sediment characteristics along the coast of North Sinai, Egypt. *Environmental geology*, *58*(7), 1419.

El-Sharnouby, B. A., El-Alfy, K.S ., Rageh, O. S., & El-Sharabasy, M. M. (2015). Coastal changes along Gamasa beach, Egypt. *Journal of Coast Zone Manag*, *17*, 393.

Hackney, C., Darby, S. E., & Leyland, J. (2013). Modelling the response of soft cliffs to climate change: A statistical, process-response model using accumulated excess energy. *Geomorphology*, *187*, 108-121.

Hwang, C. S., Choi, C. U., & Choi, J. S. (2014). Shoreline changes interpreted from multi-temporal aerial photographs and high resolution satellite images. A case study in Jinha beach. *Korean Journal of Remote Sensing*, *30*(5), 607-616.

Nassar, K., Mahmod, W. E., Fath, H., Masria, A., Nadaoka, K., & Negm, A. (2019). Shoreline change detection using DSAS technique: case of North Sinai coast, Egypt. *Marine Georesources & Geotechnology*, *37*(1), 81-95

Kermani, S., Boutiba, M., Guendouz, M., Guettouche, M. S., & Khelfani, D. (2016). Detection and analysis of shoreline changes using geospatial tools and automatic computation: Case of jijelian sandy coast (East Algeria). *Ocean & coastal management*, *132*, 46-58.

Miller, P., Mills, J., Edwards, S., Bryan, P., Marsh, S., Hobbs, P., & Mitchell, H. (2007). A robust surface matching technique for integrated monitoring of coastal geohazards. *Marine Geodesy*, *30*(1-2), 109-123.

Oyedotun, T. D. (2014). Shoreline geometry: DSAS as a tool for historical trend analysis. *Geomorphological Techniques*, *3*(2.2), 1-12.

Kuleli, T., Guneroglu, A., Karsli, F., & Dihkan, M. (2011). Automatic detection of shoreline change on coastal Ramsar wetlands of Turkey. *Ocean Engineering*, *38*(10), 1141-1149.

Thieler, E. R., Himmelstoss, E. A., Zichichi, J. L., & Miller, T. L. (2005). Digital Shoreline Analysis System (DSAS) Version 3.0: an Arcgis extension for calculating shoreline change. *United States Geological Survey, Open File Report* 2005–1304.

Thieler, E. R., & Danforth, W. W. (1994). Historical shoreline mapping (II): application of the digital shoreline mapping and analysis systems (DSMS/DSAS) to shoreline change mapping in Puerto Rico. *Journal of Coastal Research*, *10*(3).